Clays and Clay Minerals, Vol. 35, No. 1, 1–10, 1987.

DOMAIN SEGREGATION IN Ni-Fe-Mg-SMECTITES

A. DECARREAU,[1,6] F. COLIN,[2] A. HERBILLON,[3] A. MANCEAU[4,6], D. NAHON,[2] H. PAQUET,[5] D. TRAUTH-BADAUD,[1] AND J. J. TRESCASES[2]

[1] Laboratoire de Géochimie des Roches Sédimentaires, UA-CNRS 723
Université Paris XI, bât. 504, 91405 Orsay Cédex, France

[2] Laboratoire de Pétrologie de la Surface, UA-CNRS 721, Université de Poitiers
40 avenue du Recteur Pineau, 86022 Poitiers Cédex, France

[3] Groupe de Physico-Chimie Minérale et de Catalyse, Université Catholique de Louvain
Place Croix du Sud 1, 1348 Louvain la Neuve, Belgique

[4] Laboratoire de Minéralogie-Cristallographie, UA-CNRS 9, Universités Paris VI et VII
4 place Jussieu, 75252 Paris Cédex 05, France

[5] Centre de Sédimentologie et Géochimie de la Surface du CNRS
1 rue Blessig, 67084 Strausbourg Cédex, France

[6] Laboratoire pour l'Utilisation du Rayonnement Electromagnétique (LURE)
CNRS, 91405 Orsay, France

Abstract—The first stage of lateritic weathering of pyroxenes in the Niquelandia area, Brazil, leads either to Fe-rich products or to a phyllosilicate clay. In relatively unfractured parent rock the phyllosilicate clay contains Ni-rich smectites, the atomic ratio of Ni : octahedral cations ranging from 0.3 to 0.5. These smectites were studied by polarized light microscopy, X-ray powder diffraction (XRD), transmission electron microscopy, and electron microprobe, and infrared, optical absorption, Mössbauer, and extended X-ray absorption fine-structure (EXAFS) spectroscopy. The chemical composition of the smectite is constant on the optical microscope scale even to the smallest analyzed particles (3000 Å in diameter and about 75 Å thick). From XRD data the mineral is principally a swelling, trioctahedral smectite; however, some kerolite-pimelite-like layers are present, and a weak 06,33 reflection indicates the presence of a small amount of a dioctahedral phase. Mössbauer results show that all Fe cations are Fe^{3+} in octahedral sites. The structural formula of the smectite is:

$$(Ca_{0.01}K_{0.05})(Al_{0.17}Fe_{0.5}Mg_{0.48}Ni_{1.47}Cr_{0.02})(Si_{3.92}Al_{0.08})O_{10}(OH)_2$$

The results obtained from all the above methods suggest that in the smectites Ni, and, perhaps, a small amount of Mg are clustered in pimelite-like domains (or layers), whereas Fe and some Al are clustered in nontronite-like domains (or layers). Most selected-area electron diffraction patterns exhibit continuous or punctuated (*hk*) rings, indicating that particles contain several stacked layers. The patterns of some thin particles, however, suggest dioctahedral layers having trans-octahedral vacancies, such as in the Garfield, Washington, nontronite. Thus, the Ni-Fe-Mg-smectite, which seemingly is homogeneous, actually consists of mixed trioctahedral and dioctahedral layers or domains.

Key Words—Chemical composition, Laterite, Mössbauer spectroscopy, Nickel, Nontronite, Pimelite, Smectite, Transmission electron microscopy.

INTRODUCTION

Archean ultramafic rocks of Niquelandia, Goias State, Brazil, crop out as a body (40 × 2.5 km) elongated in the NNE-SSW direction. The eastern part of the body consists essentially of dunite; the western part contains a 20-m-thick lens of pyroxenitic rocks within the dunite. The Jacuba quarry (48°25′W and 14°22′S) is in the western part of the ultramafic body, which here is strongly weathered into a 30-m-thick, argillaceous and ferruginous, lateritic mantle.

Colin *et al.* (1985) reported that the chemical weathering of pyroxenes leads either to Fe-rich, noncrystalline products and then to goethite, or to a phyllosilicate clay. They showed that the phyllosilicate clay consists of either smectite in relatively unfractured parent rock or a mixture of pimelite and smectite in strongly fractured rock. Such an association of smectites and pimelite as weathering products of pyroxenes was described by Eggleton and Bolland (1982), Nahon and Colin (1982), Berner and Schott (1982), and Paquet *et al.* (1982). In the Jacuba material clays in the weathered rock are particulary enriched in Ni. Ni accounts for 33–50% of the octahedral cations of the smectites and about 85% of those in the pimelite. High Ni octahedral contents are known in the kerolite-pimelite series (Brindley *et al.*, 1979), however, Ni octahedral contents >14% (Bosio *et al.*, 1975) have not been reported before for natural smectites. Stevensites and saponites, however, having an octahedral atomic ratio Ni/(Ni + Mg) of 0 to 1 have been synthesized at low temperature (Decarreau, 1981, 1983).

In a previous paper, Colin *et al.* (1985) studied the

Table 1. Microprobe analyses of smectitic clay from poorly fractured pyroxenite rocks, Jacuba quarry, Niquelandia, Brazil.

Sample[1]	SiO_2	Al_2O_3	Fe_2O_3	MgO	CaO	K_2O	NiO	Cr_2O_3
1	55.91	5.31	10.57	4.35	0.05	0.54	22.69	0.58
2	55.14	4.75	10.33	4.44	0.04	0.38	24.21	0.70
3	54.96	1.87	6.46	3.20	0.29	0.50	32.67	0.05
4	55.07	1.62	5.77	3.51	0.12	0.52	33.24	0.19
5	54.10	2.58	8.72	6.97	0.11	0.45	26.41	0.67
6	54.80	1.83	6.11	4.81	0.17	0.35	31.66	0.67
7	55.14	3.23	13.33	5.16	0.13	0.58	25.11	0.54
8	56.42	4.83	8.71	4.13	0.09	0.47	25.13	0.22
9	58.33	1.92	16.09	5.49	0.13	0.68	16.78	0.57
10	54.84	2.12	9.77	7.98	0.05	0.53	24.13	0.60
11	55.14	1.37	12.55	4.14	0.18	0.77	25.41	0.43
12	55.10	1.89	7.30	3.10	0.13	0.48	31.76	0.23
13	56.57	2.73	15.17	2.89	0.14	0.84	20.81	0.84
14	55.52	1.68	8.01	4.32	0.08	0.58	29.55	0.26
15	56.40	4.99	8.02	4.53	0.07	0.56	25.27	0.16
16	55.94	4.48	8.79	4.99	0.13	0.56	24.92	0.19
17	56.59	3.82	10.73	5.28	0.14	0.53	22.06	0.85
18	57.13	4.90	8.86	4.00	0.10	0.61	24.71	0.31
19	53.22	4.58	10.58	6.62	0.09	0.32	23.53	1.05

[1] Samples from 1 to 18 refer to point microprobe analyses of undisturbed smectitic clay in cracks. Sample 19 is the smectitic clay extracted from weathered pyroxenes by ultrasonic methods and used for X-ray powder and electron diffraction and spectoscopic studies. Analyses were recalculated on the basis of total = 100%.

weathered pyroxenites of Jacuba by means of optical, electron microprobe, and X-ray powder diffraction techniques. The present paper describes Ni-bearing smectites formed by the weathering of Jacuba pyroxenes. One sample representative of the smectitic clay was extracted in sufficient quantity to allow its study by X-ray powder diffraction (XRD), transmission electron microscopy (TEM), infrared (IR), Mössbauer, extended X-ray absorption fine structure (EXAFS), and diffuse reflectance spectroscopy.

MATERIALS AND METHODS

Of the samples analyzed by Colin *et al.* (1985), only those extracted from poorly fractured pyroxenite rocks and which presented a smectitic clay as a weathering product were examined in the present study. Pyroxene crystals were hand picked under a binocular microscope, and the smectitic clay sample was extracted from the pyroxenes by ultrasonic cleaning and then dried and prepared for XRD, TEM, and spectroscopic analyses. The chemical composition of the extracted smectitic clay sample is in the range of point microprobe analyses of the smectitic clay (Table 1).

XRD patterns were recorded at 1°2θ/min with a CGR diffractometer equipped with a Co tube and a graphite monochromator. Scanning electron microscopy (SEM) and TEM observations were made using Jeol T200 and and JEOL 100cx microscopes, respectively. Samples were chemically analyzed with a Camebax electron microprobe using an energy-dispersive X-ray spectrometer.

Optical measurements were performed using a Cary 17D spectrophotometer equipped with a diffuse reflectance attachment. The IR spectra were obtained at ambient temperature using KBr pellets made from samples previously heated for 2 hr at selected temperatures (see Figure 4). The concentration of clay in the pellets was varied depending on the region of the spectrum to be examined and thermal treatment used. Mössbauer spectra were recorded in 512 channels of an Elscint AME 40 spectrometer in triangular mode. A ^{57}Co source in a rhodium matrix of nominal strength 25 mCi was used with NaI scintillator as a γ-ray detector. Velocity calibration was made using a high-grade metallic Fe lamina. Samples were ground with glucose to prevent preferred orientation. Because only a small amount of sample was available, spectra were accumulated to about 5×10^6 counts per channel. Only room temperature spectra were obtained. All data were computer-fitted with Lorentzian components by a least squares program.

EXAFS measurements were performed at the Ni and Fe K-edges with the synchrotron radiation at LURE-DCI (Orsay, France) (storage ring operating at 1.72 GeV and 200 mA). The X-ray beam was monochromatized with a "channel cut" Si(400) crystal. Both spectra were recorded in transmission mode from 200 eV below the absorption edge of Fe and Ni to 800 eV above, using 2-eV steps. Further experimental details are found in Raoux *et al.* (1980) and Calas *et al.* (1984). The data analysis followed the standard procedure described by Manceau and Calas (1986). EXAFS oscillations were extracted from the absorption spectrum. The resulting interference function was then Fourier transformed, yielding the radial distribution in the real space centered on the element studied. Further analysis was made by back-transforming separately each structural peak of the radial distribution function. Finally, the structural parameters were determined by a fitting procedure using the theoretical atomic scattering factors tabulated by Teo and Lee (1980). The adjusted parameters of the fit were: (1) the nature of the scatterer; (2) the interatomic distance, R; (3) the coordination number, N; (4) the mean-square distance deviation, σ (Å), related to the Debye-Waller term $\exp(-2\sigma_j^2k^2)$; and (5) the electron mean free path, Γ ($Å^{-2}$), related to the exponential dumping term $\exp(-2R_j\Gamma_j/k)$ (k = wavevector). For a particular atomic shell, N and Γ are strongly positively correlated; hence Γ was determined from reference phyllosilicates for which N is known. For R values, the use of theoretical phase shifts does not permit an accurate absolute determination of distances ($\pm$0.03 Å), but a good relative precision (better than $\pm$0.01 Å) can be obtained

https://doi.org/10.1346/CCMN.1987.0350101 Published online by Cambridge University Press

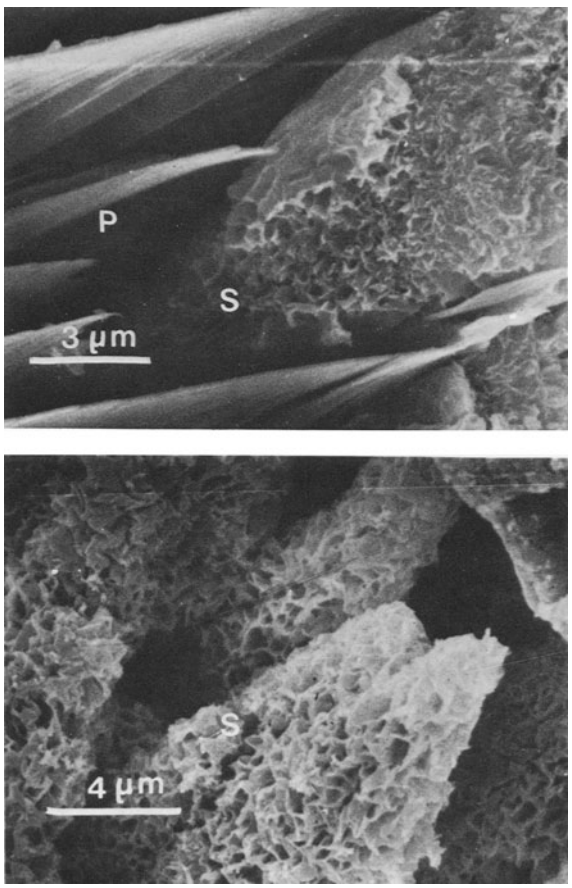

Figure 1. Scanning electron micrographs of smectitic clay sample (honeycomb structures (S)) in the weathering profiles developed on pyroxenites, Jacuba quarry, Niquelandia, Brazil: (upper) on the surface of weathered pyroxenes (P); (lower) a pseudomorph of pyroxene.

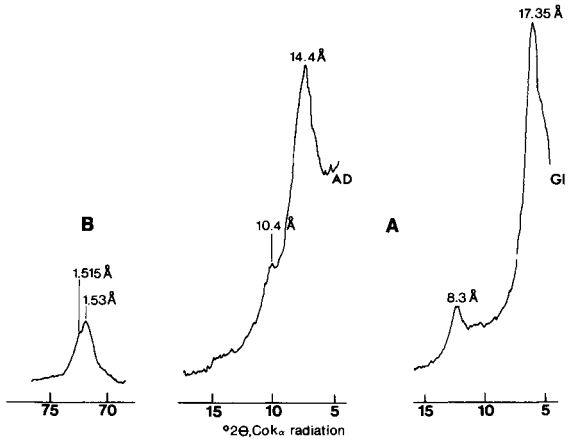

Figure 2. X-ray powder diffraction patterns of the smectitic clay sample. (A) 001 reflections of oriented aggregates (AD = air dry; Gl = glycolated); (B) 06,33 reflection from air dry powder.

by using identical procedures for the data analysis. Because scattering factors depend strongly on the atomic number of atoms, in EXAFS elements with close atomic numbers (e.g., Mg and Si or Ni and Fe) cannot be distinguished if they occur as neighboring atoms.

CHARACTERIZATION OF THE SMECTITIC CLAY

Optical microscopy

Smectitic clay was observed in thin section as 50–150-μm wide areas, apparently developed at the expense of parent pyroxenes, i.e., tightly joined enstatite (~69% of the rock) and diopside crystals (~27% of the rock). Smectite was found at grain edges and in fissures and cracks that penetrate pyroxene crystals. The weathering clay separated parent minerals into several fragments which exhibited simultaneous extinction under crossed nicols. Moreover, the smectitic clay presented an extinction parallel to the *c* axis of the original pyroxene crystal. Al these observations suggest an *in situ* weathering of parent pyroxene into smectite.

Scanning electron microscopy

Under the SEM, the clay appeared as short (about 0.5 μm) and interlocked laminae organized into honeycomb structures either on the bare surface of pyroxene (Figure 1a) or pseudomorphous after pyroxene (Figure 1b). Such structures are well known and are common in smectitic soils.

Chemical microprobe analyses

From 18 point microprobe analyses of the clay (Table 1), an average formula was calculated on the basis of $O_{10}(OH)_2$; iron is expressed as Fe^{3+}, according to Mössbauer data (see below):

$$(Ca_{0.01}K_{0.05})(Al_{0.17}Fe_{0.5}Mg_{0.48}Ni_{1.47}Cr_{0.02})$$
$$(Si_{3.92}Al_{0.08})O_{10}(OH)_2$$

This formula is unsual in that: (1) the total number of divalent cations (1.95) is low for a trioctahedral smectite, which usually contains between 2 and 2.8 divalent cations; (2) it contains 0.69 trivalent cations, whereas the upper limit for the number of R^{3+} cations in this type of octahedral sheet is generally 0.5 (Weaver and Pollard, 1973); and (3) the Al-for-Si tetrahedral substitution (0.08) is also low for a saponite, which generally contains 0.3–0.9 substitutions. Thus, this formula does not correspond to any typical smectite cited in the literature.

X-ray powder diffraction data

The XRD pattern of air-dried oriented particles shows a complex 001 reflection composed of an intense peak at 14.4 Å and a weaker peak at 10.4 Å. After saturation with ethylene glycol, a 001 peak at 17.35 Å and a 002

https://doi.org/10.1346/CCMN.1987.0350101 Published online by Cambridge University Press

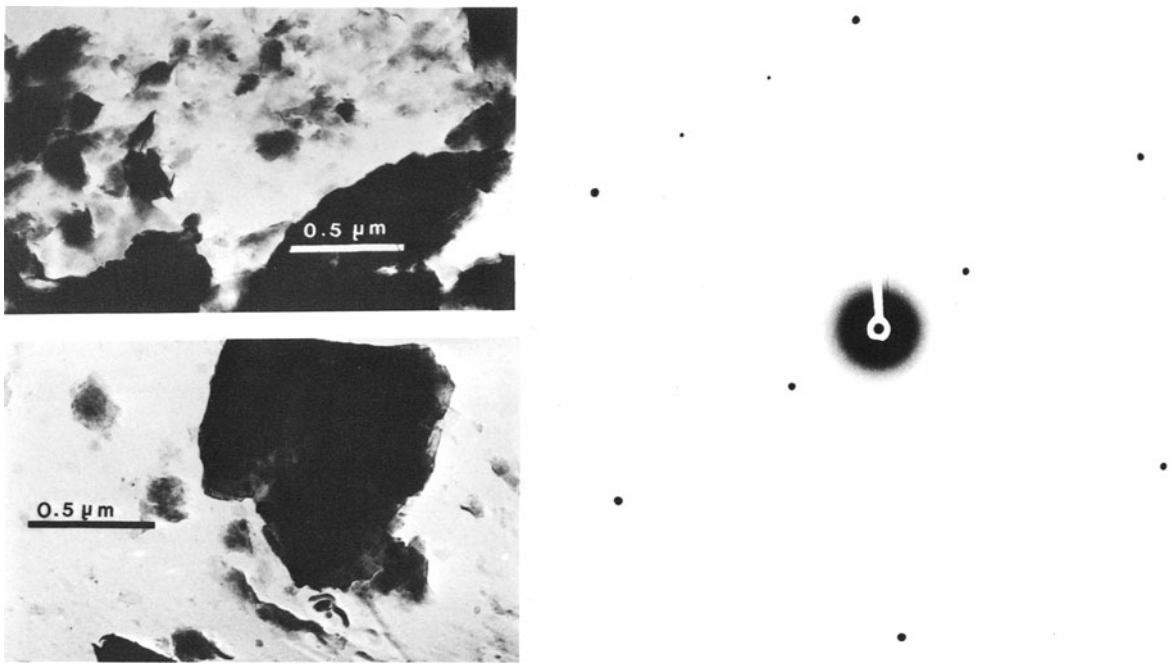

Figure 3. Transmission electron micrographs of the smectitic clay sample: (upper) isolated particles; (lower) aggregated particles; (right) selected-area electron diffraction pattern of isolated layer.

peak at 8.3 Å were visible, indicating a swelling of all the layers (Figure 2a). The layers subsequently collapsed to 9.83 Å after heating for 4 hr at 490°C. XRD patterns exhibited dissymmetric (*kh*) bands characteristic of a turbostratic stacking of layers. The 06,33 reflection presented a strong maximum at 1.53 Å and a secondary maximum at 1.51 Å (Figure 2b), leading to *b* parameter values of 9.18 and 9.06 Å, respectively. The apparent dimensions of crystal coherence, obtained using the Scherrer equation are about 90 Å in the plane of layers and 75 Å along the *c* axis (using the intense 001 reflection).

On the basis of the XRD data, the smectitic clay sample seems to consist mainly of a swelling, trioctahedral smectite; however, this identification does not take into account either the shoulder at 10.4 Å on the left flank of the major 001 reflection (Figure 2a) or the fact that the 06,33 reflection of the powder patterns also indicates the presence of a dioctahedral phase. The 10.4-Å shoulder could be due to the presence of minerals of the kerolite-pimelite series. If so, the swelling of kerolite layers (Figure 2a) could result from the small size (see below) or low crystallinity of the crystallites (Wiewiora *et al.*, 1982). These authors showed that the proportion of swelling layers in similar Ni-kerolites was increased by ultrasonic treatments.

Finally, XRD reflections similar to those displayed in Figure 2 have also been obtained on samples collected directly on the thin sections by means of microdrilling (Colin, 1984). These microsamples were X-rayed by the method described by Proust (1983).

Transmission electron microscopic observations

TEM observations showed that the smectitic clay consists of particles about 3000 Å in diameter (Figure 3a), locally forming aggregates as large as 1 μm in size (Figure 3b) and having diffuse boundaries. Chemical analyses of the 3000-Å-size particles gave peaks of Si, Mg, Al, Ni, Fe, and Cr and NiO/Fe_2O_3 ratio of 1.28–2.21, i.e., close to those obtained by electron microprobe analyses.

The smectitic clay sample was then treated ultrasonically for 5 min and diluted in distilled water to obtain single-layer particles for the electron microdiffraction. Indeed, isolated layers yielded biperiodic selected-area diffraction (SAD) patterns. Observed intensities were then directly related to the distribution of atoms in the planar cell of the layer and were not affected by interference among various layers of the clay mineral stacking. Despite ultrasonic treatment, most particles remained thick and opaque and gave continuous, broadened (*hk*) rings in SAD patterns. The few, thin observed particles were distributed among two populations. Most of the thin particles were rounded and had diameters of about 300 Å. SAD patterns showed punctuated rings suggesting that this kind of thin particle contained several stacked layers. The other few thin particles were elongated (about 100 × 500

https://doi.org/10.1346/CCMN.1987.0350101 Published online by Cambridge University Press

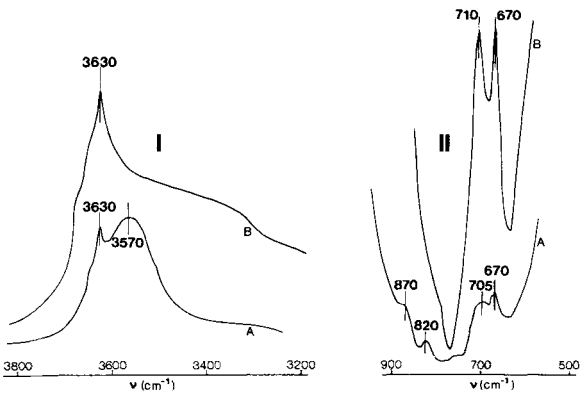

Figure 4. Infrared spectra of the smectitic clay: (A) after dehydration of the sample at 200°C under vacuum (KBr pellet; sample concentration = 2%); and (B) after partial dehydroxylation of the sample at 600°C for 2 hr (KBr pellet; sample concentration = 4%). I = 3200–3800-cm^{-1} region; II = 600–900-cm^{-1} region.

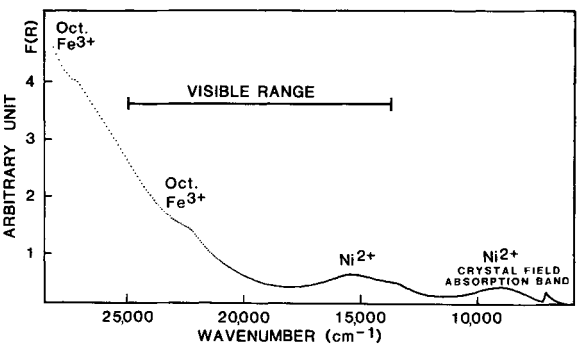

Figure 5. Optical absorption spectra of the smectitic clay sample measured in diffuse reflectance mode.

Å) and showed biperiodic diffraction patterns (Figure 3c) in which 02 reflections were as intense as 06,33, whereas the 11 and 1$\bar{1}$ reflections were very weak. This type of SAD pattern corresponds to a dioctahedral layer in which transoctahedral positions are vacant, as observed for the Garfield nontronite by Besson *et al.* (1983). TEM observations show that the smectite particles contain several layers (about 5 according to XRD results) not easily dispersed, and having predominant biperiodic, turbostratic characters. These natural free particles a few hundred Ångstroms in diameter have a chemical composition (TEM analyses) that varies in the same range as that obtained by SEM analysis of about 1 μm^3 of smectitic clay. Only after strong ultrasonic treatment of the sample were a few layers giving nontronite-like electron diffraction patterns detected.

Infrared spectroscopic results

Figure 4 presents details of the IR spectra recorded on the smectitic clay sample. In the OH-stretching region of the dehydrated sample (Figure 4-1A), two OH-stretching bands were clearly resolved. The band at 3630 cm^{-1} was at about the same frequency and had the same width as the N_D (Wilkins and Ito, 1967) OH-stretching band of Ni-talc and pimelite (Gerard and Herbillon, 1983). The band at about 3570 cm^{-1} was much broader and in the range of frequencies characteristic of the OH-stretching vibrations of nontronite (Goodman *et al.*, 1976). In the OH-bending region of the IR spectrum (Figure 4-IIA), features characteristic of both nontronite and pimelite were also noted. The 820- and 870-cm^{-1} bands were OH-bending vibrations typical of Fe-rich dioctahedral smectite, the former arising from OH groups coordinated to two Fe^{3+} ions, and the latter corresponding to the vibration of (Al,Fe^{3+})-OH groups (Serratosa, 1960; Heller *et al.*, 1962). The 705–670-cm^{-1} doublet was characteristic of talc-like, Ni-rich, trioctahedral phyllosilicates (Russell *et al.*, 1970; Brindley *et al.*, 1979).

These band assignments were further confirmed by the thermal treatment at 600°C, which destroyed all bands previously assigned to hydroxyls in a nontronite-like environment (Figure 4-IB and 4-IIB). After the heat treatment, the smectite collapsed irreversibly to 9.3 Å, and only the OH-bands characteristic for a Ni-rich talc persisted. Further, from the relative intensities of the 710–670-cm^{-1} doublet, the Ni/(Ni + Mg) ratio of the octahedral sheets in the talc-like domains in the sample was about 0.75 (Wilkins and Ito, 1967; Gerard and Herbillon, 1983).

Thus, the IR information (Figure 4) indicates that the smectite under study contained two different types of domains: one having Ni in the same local hydroxyl environment as in the octahedral sheet of pimelite, the other containing Fe^{3+} in the same environment as in the octahedral sheet of a dioctahedral Fe-rich smectite. Inasmuch as these two domains had different thermal stabilities, heating the sample at 600°C induced a dehydroxylation of the nontronite-like domains, but did not affect the domains having the same composition and the same local order as Ni-rich, talc-like phyllosilicates.

Diffuse reflectance spectroscopic results

The diffuse reflectance spectrum of the smectitic clay sample (Figure 5) consists of an intense Fe–O charge-transfer band in the ultraviolet and visible range, which partially overlaps the bands due to transitions between the 3d-orbital energy levels of Fe^{3+} and Ni^{2+}. The shoulders at 22,400 and 27,300 cm^{-1} are in the same energy region as in nontronite (Bonnin *et al.*, 1985) and are due to octahedral Fe^{3+} atoms. The two other absorption bands at lower energy are due to Ni in 6-fold coordination (Manceau *et al.*, 1985). These latter authors showed that the energy of the crystal field band at 9000 cm^{-1} depends on the type of Ni-bearing phyl-

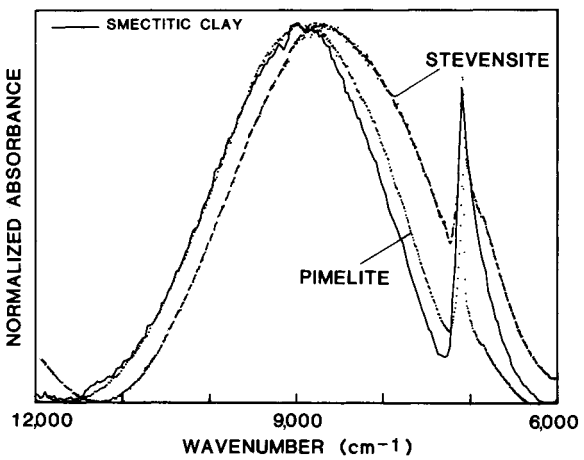

Figure 6. Normalized crystal field band from optical absorption spectra of smectitic clay sample, synthetic Ni-stevensite, and pimelite from New Caledonia.

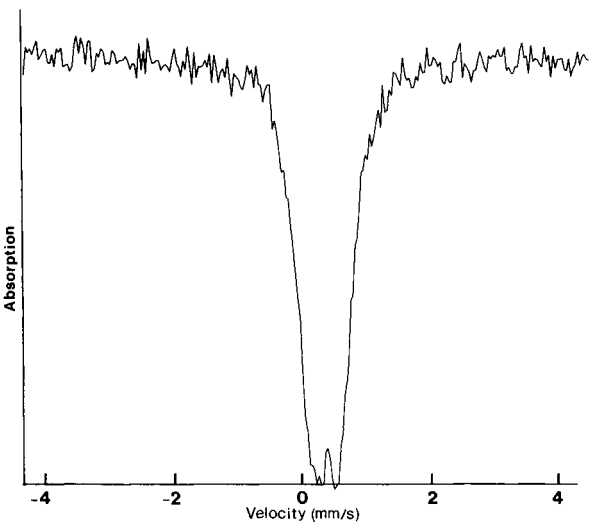

Figure 7. Mössbauer spectrum of the smectitic clay sample at room temperature.

losilicate and is independent of the Ni content. This band may thereby be used as a "fingerprint" of the Ni-containing clay mineral species. Comparing the normalized crystal field to those of pimelite and synthetic Ni-stevensite, used as reference compounds (Figure 6) the absorption maximum of the sample under study falls close to that of the pimelite and is at higher energy than that of Ni-stevensite. Thus, the Ni site is apparently *structurally* similar to that of pimelite.

Mössbauer spectroscopic results

The Mössbauer spectrum (Figure 7) of the smectitic clay sample shows only one symmetrical doublet having parameter values corresponding to Fe(III) (isomer shift = 0.352 relative to iron metal; quadrupole splitting = 0.401; peak width = 0.404; all values in mm/s). This doublet can be fitted with one Lorentzian line with an acceptable value of $\chi^2 = 1.28$.

No improvement in χ^2 was achieved by adding another doublet. Both the isomer shift (I.S.) and quadrupole splitting (Q.S.) values are typical of Fe^{3+} in cis-octahedral (M_2) sites of smectites and related minerals (Goodman *et al.*, 1976; Rozenson and Heller-Kallai, 1977; Coey, 1980; Heller-Kallai and Rozenson, 1981; Bonnin *et al.*, 1985). The peak width of the doublet is large, but still in the range of values found for equivalent doublets in Mössbauer spectra of smectites (Rozenson and Heller-Kallai, 1977; Bart *et al.*, 1980). The broadening of Lorentzian lines is due to Fe^{3+} ions located in slightly different octahedral sites having similar but not identical Mössbauer parameters. This type of result is related to crystal structures containing defects.

From Mössbauer spectra, the sample appears to contain no detectable Fe^{2+}; all ferric cations appear to be located in octahedral sites (there is no evidence of tetrahedrally coordinated Fe^{3+} ions); and most Fe^{3+} cations are located in M_2 sites.

Coey *et al.* (1984) noted that the M_2 quadrupole splitting value in 2:1 dioctahedral clay layers was broadly correlated to the decreasing Fe occupancy in the octahedral sheet. For the smectitic clay sample the Q.S. value is 0.40 mm/s, a smaller value than those of montmorillonite and beidellite (0.44–0.56 mm/s) (Rozenson and Heller-Kallai, 1977) and near those of nontronites (0.25–0.34 mm/s) (Goodman *et al.*, 1976). The Mössbauer data suggest therefore that in the smectitic clay sample under study, octahedral Fe is in an environment somewhat similar to that of nontronite.

Extended X-ray absorption fine structure spectroscopic results

Reference phyllosilicates. Successive stages of data reduction, as described above, are illustrated for Ni-talc (synthesized by B. Velde) and Garfield nontronite (sample API 33-a), taken as reference compounds (Figure 8). Because the present study involves the distribution of Ni and Fe atoms within the octahedral sheet of the smectite, only the second peak (at about 2.8 Å) of each radial distribution was investigated. The magnitude of this peak for the Ni-talc is particularly strong compared with $Ni(OH)_2$ (Manceau and Calas, 1986), so that a contribution of the four nearest Si atoms which would enhance this peak was expected. An inverse transform of this peak yielded a filtered signal (Figure 9) having a monotonic decreasing envelope which resulted from the contribution of both a 3d element (Ni) and a light element (Si). The experimental signal was simulated by a combination of Ni and Si shells (Figure 9): for the former N = 6, R = 3.00 Å, σ = 0.09 Å, Γ = 1.00 $Å^{-2}$; for the latter N = 4, R =

https://doi.org/10.1346/CCMN.1987.0350101 Published online by Cambridge University Press

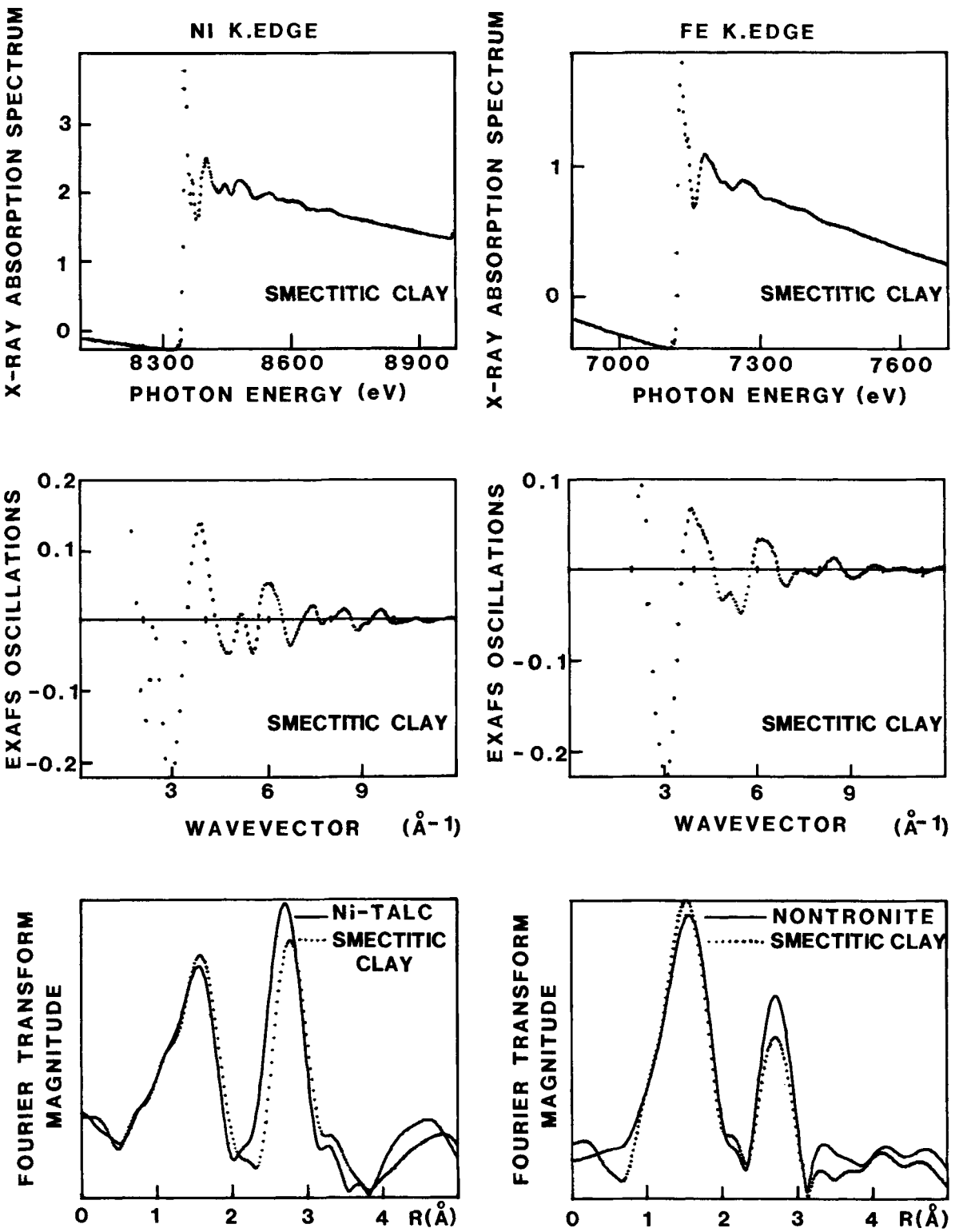

Figure 8. Successive stages of extended X-ray absorption fine structure (EXAFS) analysis at the Ni and Fe K-edge of the smectitic clay sample and reference clays (synthetic Ni-talc and Garfield nontronite). The Fourier transform (FT) was performed on the K.χ(K) function (see text). Interatomic distances are not corrected for the phase shift.

https://doi.org/10.1346/CCMN.1987.0350101 Published online by Cambridge University Press

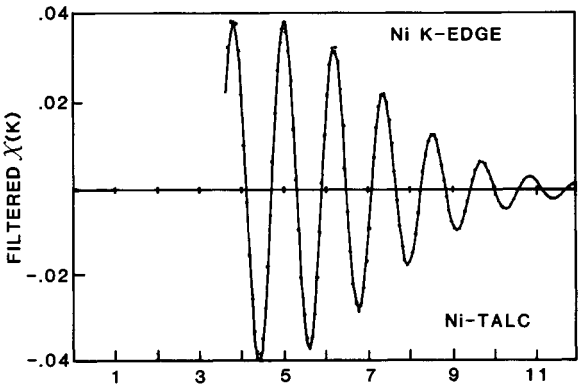

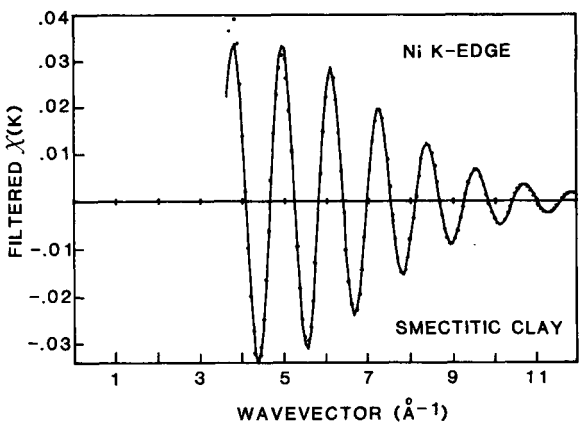

Figure 9. Filtered extended X-ray absorption fine structure (EXAFS) signal of the second peak in radial distribution at the Ni K-edge. Solid circles = experiment, continuous line = fit.

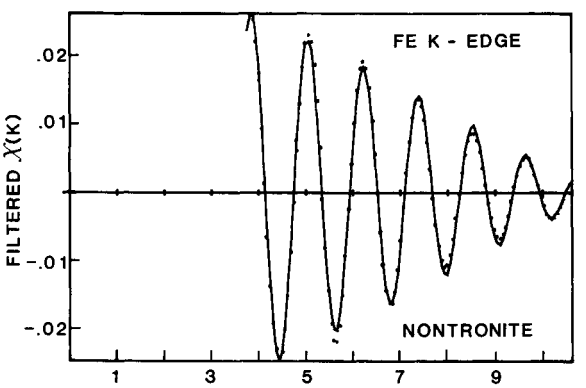

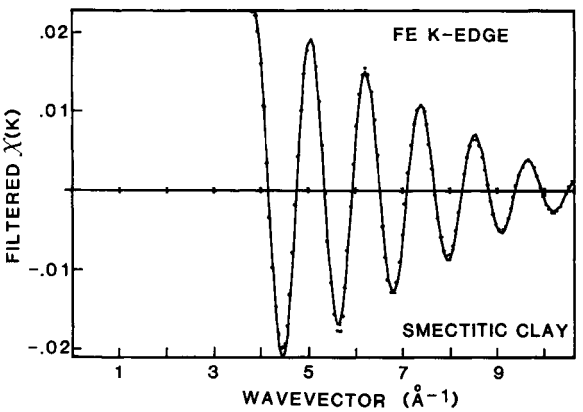

Figure 10. Filtered extended X-ray absorption fine structure (EXAFS) signal of the second peak in radial distribution at the FeK-edge. Solid circles = experiment; continuous line = fit.

3.21 Å, σ = 0.08 Å, Γ = 1.05 Å^{-2}. Like Ni-talc, the inverse transform of the second peak of nontronite yielded a partial EXAFS signal without a maximum in the envelope (Figure 10). The amplitude of the EXAFS signal was only correctly fitted in the whole k-range by assuming an additional contribution from the tetrahedral sheet. A good fit was obtained with a combination of 4 Si at 3.22 Å and 3 Fe at 3.04 Å. All parameters that were adjusted are reported in Table 2. During the fitting procedure of the partial EXAFS spectra of the smectitic clay, structural parameters relative to the tetrahedral sheet, σ and Γ, were kept constant at the values determined for the reference compounds.

Smectitic clay sample. The radial distribution functions at the Ni and Fe K-edges are compared in Figure 8 with those of the model compounds. The Fourier transform of the smectite at the Ni K-edge is close to that of the Ni-talc, which indicates a similar local order. A good fit involves 5.5 Ni(Fe) at 3.05 Å and 0.3 Mg(Al) at 3.05 Å (Figure 9, Table 2). The decreasing amplitude of the second peak in the radial structure function (Figure 8) resulted from both a slight reduction of the number of Ni second neighbors and an increase of the Ni–Ni(Fe) distance, which separates the contributions from the Ni–Si and Ni–Ni(Fe) atomic pairs.

For radial distributions around Fe, the magnitude of the second peak is clearly lower than that of a trioctahedral structure. The slight decrease of the second peak of the smectitic clay sample by comparison with that of nontronite originates either from an increase of disorder (σ) in the Fe second shell, or from a small amount of Fe–(Mg,Al) atomic pairs (waves in opposite phase). The two structural possibilities cannot be differentiated. In the former hypothesis each Fe atom is surrounded by 3 Fe atoms as in nontronite, whereas in the second one a good fit is obtained assuming a combination of 4 Si at 3.22 Å, 2.9 (Fe-Ni) at 3.04 Å, and 1.2 (Mg-Al) at 3.11 Å.

Based on the interpretation of EXAFS results, both Ni and Fe atoms are essentially surrounded by heavy atoms in the octahedral sheet of the smectitic clay sam-

https://doi.org/10.1346/CCMN.1987.0350101 Published online by Cambridge University Press

Table 2. Structural parameters of the smectitic clay and reference phyllosilicates, as determined by extended X-ray absorption fine structure (EXAFS).

Samples	Si (3rd shell)				Ni/Fe (2nd shell)				Mg/Al (2nd shell)			
	N	R (Å)	σ (Å)	Γ (Å^{-2})	N	R (Å)	σ (Å)	Γ (Å^{-2})	N	R (Å)	σ (Å)	Γ (Å^{-2})
Environment of Ni												
Synthetic Ni-talc	4.0[1]	3.21	0.08	1.05	6.0[1]	3.00	0.09	1.00				
Smectitic clay	4.0[1]	3.21[1]	0.08[1]	1.05[1]	5.5	3.05	0.09[1]	1.00[1]	0.3	3.05	0.06	1.00[1]
Environment of Fe												
Garfield nontronite	4.0[1]	3.22	0.05	2.10	3.0[1]	3.04	0.09	1.30				
Smectitic clay	4.0[1]	3.22[1]	0.05[1]	2.10[1]	2.9	3.04	0.09[1]	1.30[1]	1.2	3.11	0.05	1.30[1]

N = coordination number (±20%); R = measured distances between neighboring atoms (±0.03 Å); σ = Debye-Waller factor; Γ = mean free path of the photoelectron.
[1] Fixed parameter.

ple. The number of neighboring atoms in the second shell, however, is that of a trioctahedral sheet for Ni and of a dioctahedral sheet for Fe. Thus, from EXAFS spectroscopy both Ni and Fe ions appear to be clustered, respectively, in pimelite-like and nontronite-like domains.

SUMMARY AND CONCLUSIONS

Crystal chemistry

The microprobe and bulk analyses of the smectitic clay were similar, confirming the average structural formula of smectitic clay given above. All Fe ions are trivalent and located only in the octahedral sheet of the clay. This unusual chemical composition for a smectite appears to be the same on the microprobe scale (i.e., analyzed areas of more than 1 μm^2) to that of the smallest isolated analyzed particle (3000 Å in diameter and about 5 layers thick).

This chemical constancy contrasts with the crystal chemistry heterogeneity pointed out by different techniques. From XRD results it is clear that the smallest isolated particles visible in TEM observations are crystal mosaics, inasmuch as coherent *domains* in the (*a,b*) plane are less than 100 Å in diameter. Similarly, all spectroscopic methods show atom segregations into pimelite-like domains rich in Ni and nontronite-like domains rich in Fe. Furthermore, from EXAFS results Ni and Fe atoms are clustered in domains having minimum diameters of about 30–40 Å (Manceau and Calas, 1986). Domain size can therefore be as large as the maximum dimension of the mosaic crystals, i.e., 100 Å.

Few data are available for the lighter elements such as Mg and Al. IR data suggest that part of the Al is associated with Fe in dioctahedral nontronite-like domains, whereas small amounts of Mg(Al) occur as neighboring ions in Ni- and Fe-clusters (EXAFS results). Hence, it is impossible to describe more accurately the actual location of these atoms in the clay structure.

The heterogeneity of the particles can result from various spatial distributions of the domains; e.g., the domains of segregation may be in the same layer or in alternate layers. If octahedral cations are completely segregated in separated di- and trioctahedral layers, the structural formula of the smectitic clay would be:

$$\tfrac{2}{3}[Si_4Mg_{0.74}Ni_{2.26}O_{10}(OH)_2] + \tfrac{1}{3}[(Si_{3.77}Al_{0.23})(Al_{0.5}Fe_{1.45}Cr_{0.07})O_{10}(OH)_2],$$

which shows that dioctahedral domains (or layers) represent one third of the sample. The XRD results indicate that the smectitic clay is mainly trioctahedral, and the TEM observations disagree with the possibility of a mechanical mixing of two populations (one trioctahedral, and other dioctahedral) of clay particles, each containing several stacked layers. The observation of isolated nontronite-like particles suggests that the smectitic clay contains mixed trioctahedral/dioctahedral layers; however, juxtaposition of Ni-domains and Fe-domains within the same layer cannot be completely excluded. Furthermore, because of the minimum mean size of the Ni-clusters, mixed pimelite-Mg-smectite-nontronite layers may be present.

Moreover, segregated layers and/or domains exhibit some uncommon features. Ion domains (layers) are not strictly nontronite, as shown by Mössbauer spectroscopy. In fact, only one doublet for octahedral Fe was found in the spectrum of the sample studied, whereas two doublets have generally been observed for nontronite and attributed to Si-M^{3+} tetrahedral substitutions (Goodman, 1978; Besson *et al.*, 1983) or poorly crystallized regions (Bonnin *et al.*, 1985). The most important feature is connected with Ni domains. Both IR and diffuse reflectance spectra show that Ni is located in pimelite-like octahedral sites. By XRD some kerolite layers appear to be present, but most of the layers, however, are those of swelling smectites. The swelling of these layers can be explained both by the small size of particles and/or by a disordered turbostratic lacking of pimelite and nontronite-like layers.

Genetic implications

From petrographic studies Colin (1984) showed that the first stage of the weathering of the Jacuba quarry

https://doi.org/10.1346/CCMN.1987.0350101 Published online by Cambridge University Press

pyroxenes was controlled by the degree of fissuring of the bed-rock. He found smectite containing about 50% Ni in the octahedral layer (the smectitic clay of this study) in relatively unfractured parent rock. In highly fractured rock he reported a mixture of smectite (Ni 33%) and pimelite (Ni 85%).

The present crystal chemical study of the smectitic clay shows that this distinction is only a matter of the observation scale. Smectite particles 3000 Å in diameter consist of both Ni-rich pimelite-like domains (or layers) and of Ni-free nontronite-like domains (or layers). As the degree of fissuring increases, the particles of pimelite separate from ferric-smectite particles. Subsequently, pimelite particles coalesce to form progressively larger, centimeter-size aggregates.

ACKNOWLEDGMENTS

The authors thank the staff of LURE for synchrotron facilities and E. Merino for English improvement.

REFERENCES

Bart, J. C., Burriesci, N., Cariati, F., Micera, G., and Gessa, C. (1980) Spectroscopic investigation of iron distribution in some bentonites from Sardinia: *Clays & Clay Minerals* **28,** 233–236.

Berner, R. A. and Schott, J. (1982) Mechanisms of pyroxene and amphibole weathering. II. Observations of soil grains: *Amer. J. Sci.* **282,** 1214–1231.

Besson, G., Bookin, A. S., Dainyak, L. C., Rautureau, M., Tsipursky, S. I., Tchoubar, C., and Drits, U. A. (1983) Use of diffraction and Mössbauer methods for the structural and crystallochemical characterization of nontronite: *J. Appl. Crystallogr.* **16,** 374–383.

Bonnin, D., Calas, G., Suquet, H., and Pezerat, H. (1985) Intracrystalline distribution of Fe^{3+} in Garfield nontronite: A spectroscopic study: *Phys. Chem. Minerals* **12,** 55–64.

Bosio, N. J., Hurst, V. J., and Smith, R. L. (1975) Nickeliferous nontronite, a 15 Å garnierite, at Niquelandia, Goias, Brazil: *Clay Miner.* **23,** 400–403.

Brindley, G. W., Bish, D. L., and Wan, H. M. (1979) Compositions, structure and properties of nickel-containing minerals in the kerolite-pimelite series: *Amer. Mineral.* **64,** 615–625.

Calas, G., Basset, W. A., Petiau, J., Steinberg, M., Tchoubar, D., and Zarka, A. (1984) Mineralogical applications of synchrotron radiation: *Phys. Chem. Minerals* **11,** 17–36.

Coey, J. M. D. (1980) Clay minerals and their transformations studied with nuclear techniques: The contribution of Mössbauer spectroscopy: *Atomic Energy Review* **18,** 73–124.

Coey, J. M. D., Chukhrov, F. V., and Zvyagin, B. B. (1984) Cation distribution, Mössbauer spectra and magnetic properties of ferri-pyrophyllite: *Clays & Clay Minerals* **32,** 198–204.

Colin, F. (1984) Etude pétrologique des altérations de pyroxénite du gisement nickellifère de Niquelândia (Brésil): *Thèse 3è cycle, Univ. Paris VII,* Paris, 136 pp.

Colin, F., Noack, Y., Trescases, J. J., and Nahon, D. (1985) L'altération latéritique débutante des pyroxénites de Jacuba, Niquelândia, Brésil: *Clay Miner.* **20,** 93–113.

Decarreau, A. (1981) Cristallogenèse à basse température de smectites trioctaédriques par vieillissement de coprécipités silicométalliques: *C.R. Acad. Sci. Paris D* **292,** 61–64.

Decarreau, A. (1983) Etude expérimentale de la cristallogenèse des smectites. Mesures des coefficients de partage smectite trioctaédrique-solution aqueuse pour les métaux M^{2+} de la première série de transition: *Sci. Géol. Mém.* **74,** 1–185.

Eggleton, R. A. and Bolland, J. W. (1982) Weathering of enstatite to talc through a sequence of transitional phases: *Clays & Clay Minerals* **30,** 11–20.

Gerard, P. and Herbillon, A. J. (1983) Infrared studies of Ni-bearing clay minerals of the kerolite-pimelite series: *Clays & Clay Minerals* **31,** 143–151.

Goodman, B. A. (1978) The Mössbauer spectra of nontronites: Consideration of an alternative assignment: *Clays & Clay Minerals* **26,** 176–177.

Goodman, B. A., Russell, J. D., Fraser, A. R., and Woodhams, F. W. D. (1976) A Mössbauer and IR spectroscopic study of the structure of nontronite: *Clays & Clay Minerals* **24,** 53–59.

Heller, L., Farmer, V. C., Mackenzie, R. C., Mitchel, B. D., and Taylor, H. F. W. (1962) The dehydroxylation and rehydroxylation of trimorphic dioctahedral clay minerals: *Clay Miner. Bull.* **5,** 56–72.

Heller-Kallai, L. and Rosenson, I. (1981) The use of Mössbauer spectroscopy of iron in clay mineralogy: *Phys. Chem. Minerals* **7,** 223–238.

Manceau, A. and Calas, G. (1986) Nickel-bearing clay minerals. 2. X-ray absorption study of Ni-Mg distribution: *Clay Miner.* **21,** 341–360.

Manceau, A., Calas, G., and Decarreau, A. (1985) Nickel-bearing clay minerals. I. Optical study of nickel crystal chemistry: *Clay Miner.* **20,** 367–387.

Nahon, D. and Colin, F. (1982) Chemical weathering of orthopyroxenes under lateritic conditions: *Amer. J. Sci.* **282,** 1232–1243.

Paquet, H., Duplay, J., and Nahon, D. (1982) Variations in the composition of phyllosilicate monoparticles in a weathering profile of ultrabasic rocks: in *Proc. Int. Clay Conf., Bologna, Pavia, 1981,* H. van Olphen and F. Veniale, eds., Elsevier, Amsterdam, 595–603.

Proust, D. (1983) Mécanisme de l'altération supergène des roches basiques. Etudes des arènes d'orthoamphibolites du Limousin et de glaucophanite de l'île de Groix, Morbihan: *Thèse Sci., Univ. Poitiers,* France, 197 pp.

Raoux, D., Petiau, J., Bonnot, P., Calas, G., Fontaine, A., Lagarde, P., Levitz, P., Loupias, G., and Sadoc, A. (1980) L'EXAFS appliqué aux déterminations structurales de milieux désordonnés: *Rev. Phys. Appl.* **15,** 1079–1094.

Rozenson, I. and Heller-Kallai, L. (1977) Mössbauer spectra of dioctahedral smectites: *Clays & Clay Minerals* **25,** 94–101.

Russell, J. D., Farmer, V. C., and Velde, B. (1970) Replacement of OH by OD in layer silicates and identification of the vibrations of these groups in infrared spectra: *Mineral. Mag.* **37,** 870–879.

Serratosa, J. M. (1960) Dehydratation studies by IR spectroscopy: *Amer. Mineral.* **45,** 1101–1104.

Teo, B. K. and Lee, P. A. (1980) *Ab initio* calculation of amplitude and phase function for extended X-ray absorption fine structure (EXAFS) spectroscopy: *J. Amer. Chem. Soc.* **101,** 2815–2830.

Weaver, C. E. and Pollard, L. D. (1973) *The Chemistry of Clay Minerals:* Elsevier, Amsterdam, 213 pp.

Wiewiora, A., Dubinska, E., and Iwasinska, I. (1982) Mixed-layering in Ni-containing talc-like minerals from Szklary, Lower Silesia, Poland: In *Proc. Int. Clay Conf., Bologna, Pavia, 1981,* H. van Olphen and F. Veniale, eds., Elsevier, Amsterdam, 111–126.

Wilkins, R. W. T. and Ito, J. (1967) Infrared spectra of some synthetic talcs: *Amer. Mineral.* **52,** 1649–1661.

(Received 20 February 1986; accepted 3 September 1986; Ms. 1565)